Feature-based detection of landmines in infrared images

Wilhelmus A. C. M. Messelink[ab] Klamer Schutte[b], Albert M. Vossepoel[a]
Frank Cremer[bac], John G. M. Schavemaker[b], Eric den Breejen[b]

[a]Pattern Recognition Group, Delft University of Technology, Delft, The Netherlands
[b]TNO Physics and Electronics Laboratory, P.O. Box 96864, 2509 JG, The Hague, The Netherlands
[c]Section of Applied Geophysics, Delft University of Technology, Delft, The Netherlands

ABSTRACT

High detection performance is required for an operational system for the detection of landmines. Humanitarian de-mining scenarios, combined with inherent difficulties of detecting landmines on an operational (vibration, motion, atmosphere) as well as a scenario level (clutter, soil type, terrain), result in high levels of false alarms for most sensors. To distinguish a landmine from background clutter one or more discriminating object features have to be found.

The research described here focuses on finding and evaluating one or more features to distinguish disk-shaped landmines from background clutter in infrared images. These images were taken under controlled conditions, with homogenous soil types.

Two methods are considered to acquire shape-based features in the infrared imagery. The first method uses a variation of the Hough transformation to find circular shaped objects. The second method uses the tophat filter with a disk-shaped structuring element. Furthermore, Mahalanobis and Fisher based classifiers are used to combine these features.

Keywords: landmine detection, infrared, Hough transform, tophat filter, feature selection

1. INTRODUCTION

Thermal infrared cameras often are used to detect landmines.[1–3] In this paper we applied the Hough transform and the tophat filter to the IR images of surface laid and buried anti-personnel landmines. Both methods have been optimized with regard to three different cost functions, resulting in optimal working point selection. In addition a feature-based detection of the landmines is introduced. As features we used the results of the Hough transform and tophat filter as optimized for the three working points. The feature combination methods used are based on the Manahalobis distance and the Fisher mapping. Exhaustive search was applied to find the optimal feature combinations.

In the next section the theoretical foundation is given for the various parts of the infrared landmine detection algorithms. Section 3 gives the experimental results obtained on the LOTUS data sets. Finally, conclusions and a discussion will be given.

2. THEORY

Using thermal infrared images to detect landmines is based on the assumption that landmines have different thermal properties than their surrounding soil.[4] When an area is heated due to solar radiation, the landmines will warm up quicker than the soil. When a landmine is buried, the soil above it warms up quicker, because of the thermal properties of the landmine. The influence of the landmine on the temperature of the soil at surface level relates to the burial depth. This situation, where landmines give relatively warm spots at the surface, is called a situation with positive contrast.

When an area is cooled (for instance some time after sunset) the situation is reversed. Landmines will cause cold spots at the surface and this situation is called to have negative contrast. As follows from the previous, the contrast of a particular moment in time is determined by meteorological factors and can therefore be predicted at the time of measurement with an appropriate thermal model.[5,6]

So an indication for the presence of landmines is difference in local thermal contrast. However, there is a natural variation of thermal contrast due to inhomogeneities in the background (soil type variations, variations in soil height, other objects, etc.) The variations not caused by the presence of landmines are called clutter. To reduce the false alarms caused by clutter,

Further author information: (Send correspondence to Klamer Schutte)
Klamer Schutte: E-mail: Schutte@fel.tno.nl Phone: +31 70 374 0469 Fax: +31 70 374 0654

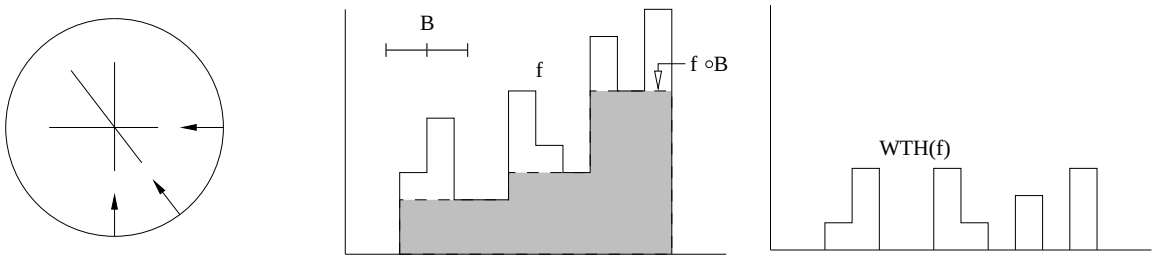

Figure 1. An example of the Hough transform (a) and the tophat filter (b) and (c). For the Hough transform, the three arrows depict the orientation of the gradient of three points that have a magnitude of the gradient that is greater than the threshold level. If the gradients are oriented perpendicular to the circle through the points the lines drawn coincide in the center of the circle. For an 1D signal as shown in (b) the morphological opening is depicted by the gray area. The resulting white tophat filter is given in (c).

more information needs to be taken into account. The focus for this paper is be on shape features. The image features under investigation here are modified versions of the Hough transform and the tophat filter. These methods are implemented such that they result in confidence values. A confidence value is a monotonic increasing function of the probability of a landmine present at it's defined location. These confidence values are computed for both methods on a predefined spatial grid over the area under investigation.

The confidence levels are used to classify (landmine or background) the data by assigning grid cells with confidence values above the detection-threshold, t, to the landmine class ($D = M$), and values below to the background ($D = \bar{M}$). Increasing the threshold reduces the number of false alarms, but also leads to a lower detection rate. The confidence values are subsequently used as input for a feature selection process

2.1. Hough transform

The Hough transform is a method to find shapes in images.[7] The first step is to find the edges in the images. To find the edges in the images, we use a Gaussian gradient filter.[8] The Hough transform uses voting: each edge pixel gives a vote to each shape it can be a part of. Each possible shape is represented by a bin in accumulator space, of which each dimension represents a parameter of the shape under investigation. When a bin in accumulator space acquires relatively many votes, the original image contains a shape with the corresponding parameters.

Since we are looking for disk-shaped landmines and have a vertical imaging geometry, the shape template used is a circle. For a disk-shaped landmine with positive contrast the gradient on its edge points towards the center of the landmine and simultaneous the magnitude of this gradient is higher than the average magnitude of the gradient in the background.

We use this information to obtain the edge by thresholding the magnitude of the gradient. Next, in accumulator space we add lines in the direction of the gradient (or in the opposite direction for negative contrast landmines). Where lines coincide the values are added.

The lines start at a certain distance from the edge points and have a finite length. These properties are determined by the minimum and maximum expected radii of the landmines. Furthermore, the value of the line is normalized as landmines with bigger radii are expected to have larger amounts of edge pixels. An example of this procedure is given in Figure 1(a).

The resulting accumulator space is mapped to a confidence value on the desired grid. This is performed by spatially re-scaling the image while preserving local maximum, followed by a morphological maximum filter with a square structuring element. The size of this filter is a parameter of this method. Other tunable parameters are the kernel size of the gradient filter and the magnitude at which the gradient is thresholded. The detection threshold value is the final parameter needed to convert confidence data into a detection decision. Each setting of those four parameters provides a certain number of detected landmines and false alarms. ROC curves, where the detection rate is plotted versus the false alarm rate,[9] are shown in Figure 2 where each point on each curve corresponds with a unique parameter setting. It can be seen that there exists no ROC curve which provides best performance for all points.

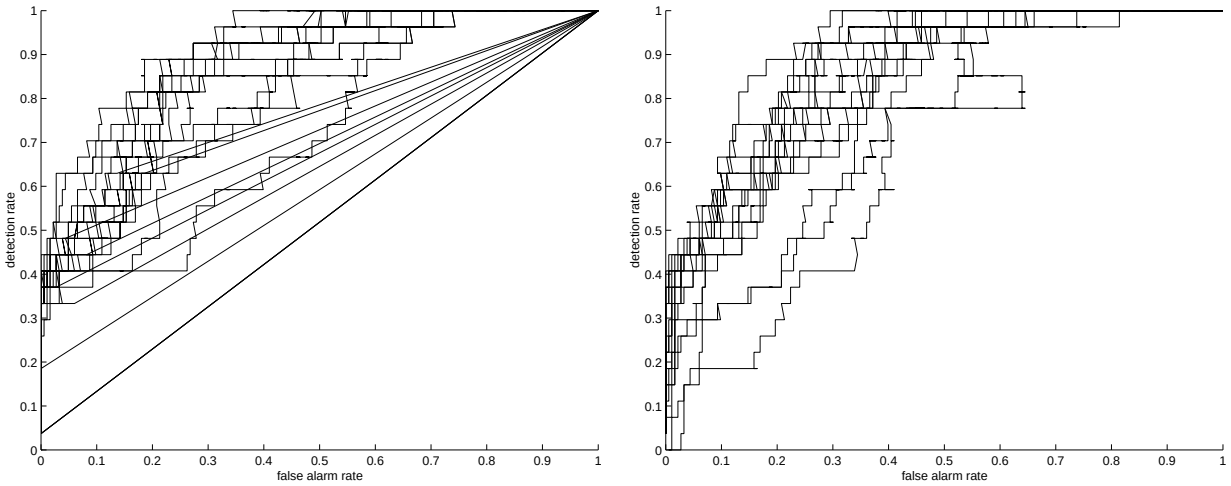

Figure 2. In (a) the influence of the Hough transform parameters (the kernel size of the gradient filter, between 4.65 and 37.21 mm, the gradient at which the gradient is thresholded, between 0.023 and 23.26 and the size of the structuring element of the morphological maximum filter, between 13.95 and 32.56 mm) on the detection and the false alarm rate is shown as ROC curves. In (b) the same is shown for the parameters of the tophat filter (the kernel size of the Gaussian blurring filter, between 0 and 41.86 mm, the size of the structuring element of the tophat filter, between 23.26 and 232.56 mm and the size of the structuring element of the morphological maximum filter, between 13.96 and 32.56 mm). One out of ten used parameter settings is plotted for reasons of separability.

2.2. Tophat filter

The tophat algorithm is a morphological transform that is used to extract either locally bright (warm) or locally dark (cold) objects, with the use of shape information and relative brightness.[10] For the situation with positive contrast the white tophat filter is used. This transformation on an image is defined as:

$$WTH(f) = f - f \circ B$$

where $f \circ B$ denotes a morphological opening operator for gray-scale images with a structuring element B, which removes image structures that are smaller than B. By subtracting the result of the opening from the original image we obtain those structures smaller then B. Therefore, the size of the structuring element of the opening determines the maximum size of objects extracted with the tophat filter. The structuring element B is a disk with a selectable radius. For situations with negative contrast the *black* tophat filter is used, which is defined as:

$$BTH(f) = f \bullet B - f$$

Here, $f \bullet B$ denotes a morphological, gray-scale closing with structuring element B. An example of the white tophat filter is shown in Figures 1(b) and 1(c).

Before we apply the tophat algorithm, a Gaussian blurring filter[11] is applied to the images to reduce the influence of noise. Similar to the Hough algorithm, after applying the tophat filter on these filtered images, the result is mapped to a confidence level on the predefined grid, by re-scaling and applying a morphological maximum filter. This results in three parameters for the tophat algorithm, namely the kernel size of the Gaussian blurring, the radius of the structuring element B and the kernel size of the morphological maximum filter.

2.3. Performance evaluation

The performance of different techniques is expressed using the probability of detection P_d and the probability of false alarm P_d, defined as:

$$P_d = P(D = M|M)$$
$$P_{fa} = P(D = M|\bar{M})$$

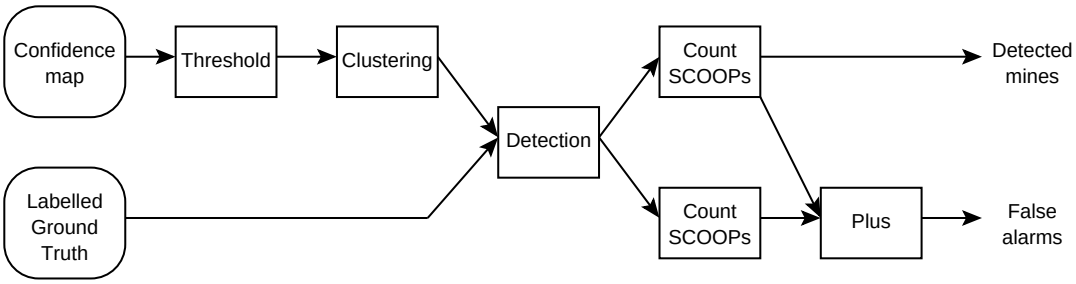

Figure 3. The flowchart of SCOOP evaluation method. The input of this evaluation method is a confidence map and a ground truth. This evaluation method returns the number of detected landmines as well as the number of false alarms with a predefined maximum SCOOP size.

However, calculating these values is not straightforward, since the processed measurements are on a grid that has spatial correlation. For instance, a single landmine might be represented by several (connected) pixels in the measurement data. To detect the landmine it is sufficient if only one of these measurements generates a detection.

The same applies for false alarms, connected measurements that generate a false detection should not be penalized similar to an equal amount of spatially separated false detections. If one does not take this effect into account, one overestimates the probability of false alarm. On the other hand, extremely large false alarm areas should be penalized more as they involve more work in verifying with other means.

To remedy these effects, we used the SCOOP[12] method, which yields less biassed probabilities by taking into account the spatial arrangement. An overview of the method is given in Figure 3. In essence, the SCOOP method counts spatial clusters of false-positives as one false alarm, unless the size of the cluster is larger than a certain size (the SCOOP-size). In that case the cluster counts as multiple false alarms, namely, as the number of times a SCOOP-sized area fits in the area of the cluster. A cluster partially covering the ground truth area of an object counts as a proper detection.

2.4. Work point selection

For each specific cost function, which incorporates the cost of a missed detection and the cost of a false alarm.The optimal parameter setting is determined by minimizing the cost over all parameter settings. The minimal cost for a cost function can be compared between different detection schemes. We define our cost function as follows: $C_{\bar{M}|M} = C(D = \bar{M}|M)$ is the cost for classifying a landmine as background (missed detection) and $C_{M|\bar{M}} = C(D = M|\bar{M})$ is the cost for classifying background as a landmine (false alarm). The cost of correctly classified background or landmines are thought to be non-existent.

When we define $P(M)$ and $P(\bar{M})$ as the *a priori* probability a grid cell belongs to the landmine or background class respectively, the expected cost of applying the classifier represented by a point (P_{fa}, P_d) in ROC space is[13] :

$$P(M) \cdot (1 - P_d) \cdot C_{\bar{M}|M} + P(\bar{M}) \cdot P_{fa} \cdot C_{M|\bar{M}}$$

Therefore, two points, $(P_{fa,1}, P_{d,1})$ and $(P_{fa,2}, P_{d,2})$, have the same performance if

$$\frac{P_{d,2} - P_{d,1}}{P_{fa,2} - P_{fa,1}} = \frac{C_{M|\bar{M}} P(\bar{M})}{C_{\bar{M}|M} P(M)}$$

This equation defines an *iso-performance line*, i.e. all classifiers corresponding to points on the line have the same expected cost. Lines closer to the top-left of the ROC space - having a larger detection rate intercept - are better as they correspond to a classifier with lower expected cost.

To minimize expected cost it suffices to find that point in the ROC space that lies on the most ”top-left” iso-performance line. This implies that if a point does not lie on the convex hull of the set of points in the ROC space, then for any family of iso-performance lines, i.e. for any cost function, there is another point that lies on a better iso-performance line, and thus the associated classifier can never be optimal with regard to expected cost. To represent the performance of different techniques it therefore is sufficient to plot the convex hull of the set of ROC points of each technique.

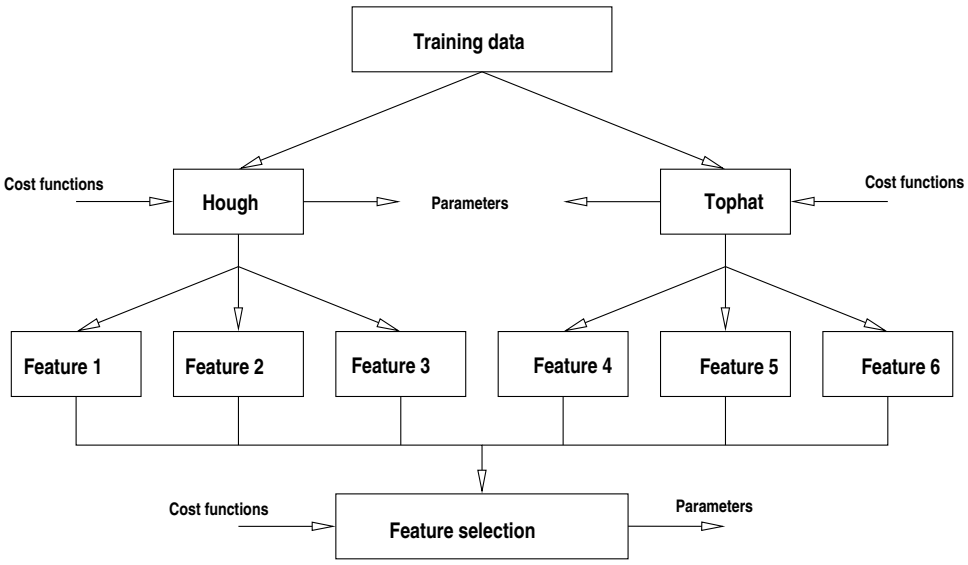

Figure 4. Flowchart of the Feature selection process. Using three cost functions, three parameter settings of both the Hough transform as the tophat filter are selected. The resulting confidence values serve as features in a Feature selection process.

2.5. Benefit function

The performance envelope of a detection system is fully determined by its ROC curve. However, these curves are sometimes difficult to interpret, as they take into account all possible operating points. Furthermore, for an operational system one operating point has to be selected. The cost function as defined above is normalized, resulting in a benefit function.[14] The normalization is performed such that unity benefit represents a perfect system with no errors. Zero benefit represents the best a priori choice either no-detections and no-false alarms, or 100% detections and 100% false alarm. In mathematical form this benefit is:

$$b = 1 - \frac{P(M) \cdot (1 - P_d) \cdot C_{\bar{M}|M} + P(\bar{M}) \cdot P_{fa} \cdot C_{M|\bar{M}}}{P(M) \cdot C_{\bar{M}|M}}$$

when normalizing to the no-detections and no-false alarms point, and:

$$b = 1 - \frac{P(M) \cdot (1 - P_d) \cdot C_{\bar{M}|M} + P(\bar{M}) \cdot P_{fa} \cdot C_{M|\bar{M}}}{P(\bar{M}) \cdot C_{M|\bar{M}}}$$

when normalizing to the 100% detections and 100% false alarms point. Note that actual systems might deliver negative benefit. This means that, given the cost metric, one would achieve better performance with switching the system off and using the best *a priori* estimate.

2.6. Feature selection and combination

In this section the feature selection and combination process is outlined. For both the Hough and tophat method we use three parameter settings. To do this we optimize these methods for three benefit functions. The first benefit function results from a cost function that is derived from practical restraints. Here, the cost of one false alarm per square meter equals a 10 percent decrease in detection rate.[15] Benefit function A is this cost function normalized using the procedure outlined above. The benefit functions B and C result from multiplying the relative cost of a missed landmine by a factor of 10 and 0.1 respectively and then normalizing these cost functions. For both benefit functions A and B normalization is performed on the no-detections and no-false alarms point, for benefit function C the 100% detections and 100% false alarms point is used.

We utilize the confidence levels from both the Hough and tophat methods, using the parameter settings thus found, as features. The three benefit functions per method lead to a total of six features. From these six features we try all combinations and evaluate the performance of these combinations. Using this exhaustive search we find the best performing combination of features. This is achieved by mapping the n-dimensional (where n is the number of features used in the combination under

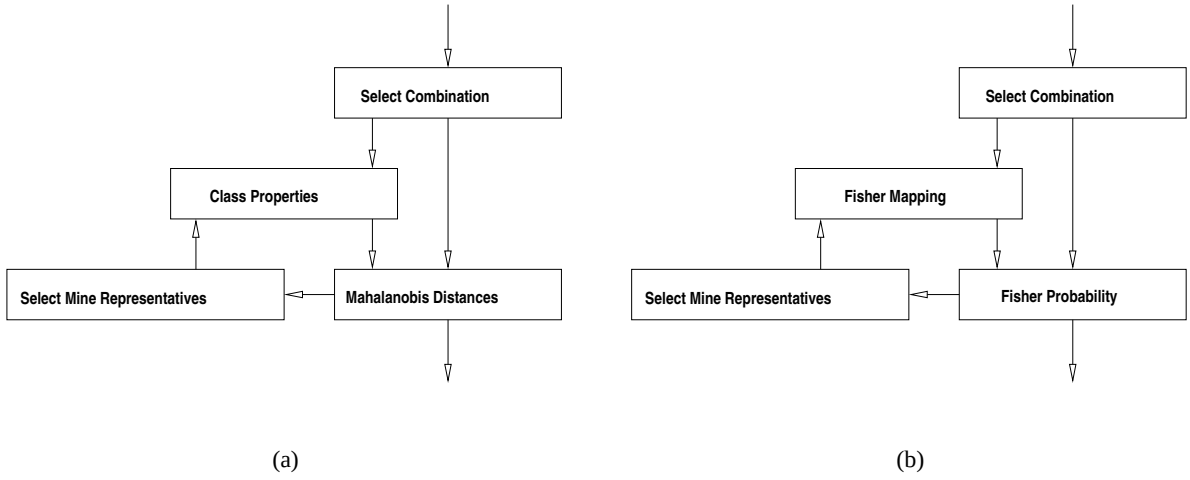

(a) (b)

Figure 5. Flowcharts of the Mahalanobis (a) and Fisher (b) combination methods

investigation) feature space onto an one dimensional confidence level, comparable to that of the Hough and tophat methods. An overview is shown in Figure 4. Two mapping methods are considered, Mahalanobis distances and Fisher probabilities.

Because there is a small uncertainty in the position of the landmines in the training data, the ground truth for each landmine encompasses a larger area then the actual area of the landmines. This means that in the ground truth some grid cells are incorrectly labelled as landmine. This leads to an error in the estimated parameters of the distribution of the landmine class, used by both the Mahanalobis and Fisher classifiers. To improve the estimates of the parameters of the landmine class we condense the training data for each landmine to one point, namely that grid cell providing the highest confidence level. Using this reduced set of training data, the parameters of this distribution of the landmine class are recalculated, leading to new confidence levels. With these new confidence values, again a new representing point for each landmine is computed, leading to an iterative process in which an optimal estimation of the parameters of the distribution of the landmine class are obtained. An overview of this method is shown in Figure 5(a) and 5(b).

2.6.1. Mahalanobis distances

Using labelled data, the two classes (background and landmines) are modelled as normally distributed and the parameters (mean and covariance) are estimated. Using these parameters the Mahalanobis[16] distances to each class mean can be computed for each point in the feature space. We define the resulting confidence level for a grid cell as the distance to the background class divided by the distance to the landmine class.

2.6.2. Fisher mapping

The second mapping under consideration is the based on the Fisher mapping.[16] Using Fisher mapping a linear classifier is produced utilizing the training data. This classifier gives us an estimation of the probability that a grid cell belongs to the landmine class. These probabilities are the output confidence levels of the mapping. One of the difference between the Mahalanobis distance and the Fisher mapping is that the latter can use a single feature values as it's resulting confidence values.

3. EXPERIMENTAL RESULTS

3.1. Description of the data used

The test facility[1] used in the experiments is located outdoors and consist of multiple lanes, measuring 3×10 m^2, with each a different soil type. We used data recorded on four of the six lanes: the sand, clay, peat and ferruginous ones, shown in Figure 6. The use of the TNO-FEL test lanes ensure constant soil type and ground water level within each of these lanes. The data used in this experiment was recorded in January 2001 with an Radiance HS camera. This camera operates in the midwave infrared band (MWIR) and has a focal plane array of 256×256 pixels^2. The imaging geometry used resulted in pixels of 4.65 mm^2 on the ground. For the for surface laid landmines, the meteorological conditions and time of day during image capture resulted in

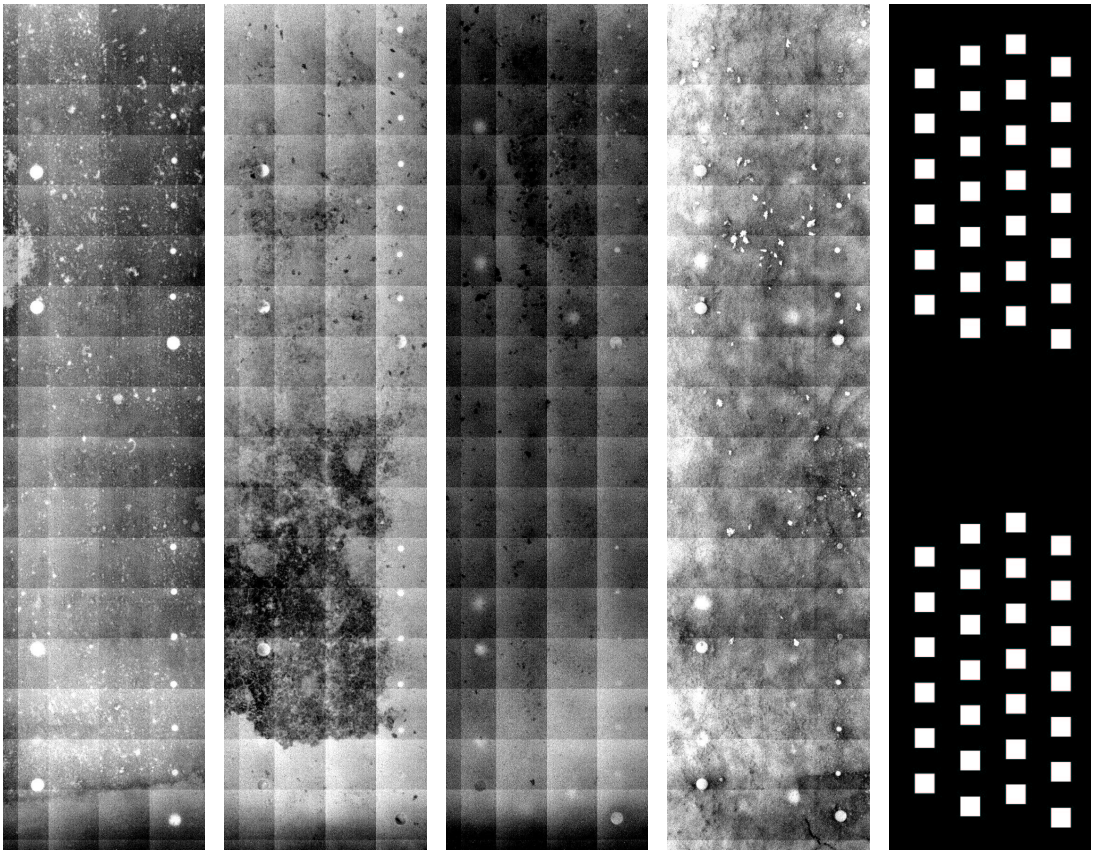

(a) (b) (c) (d) (e)

Figure 6. Mosaics of the images used. From left to right depicted are the sand, clay, peat, ferruginous lanes and the ground-truth positions for landmine object in these lanes. The ferruginous lane is shown inverted because it has negative contrast.

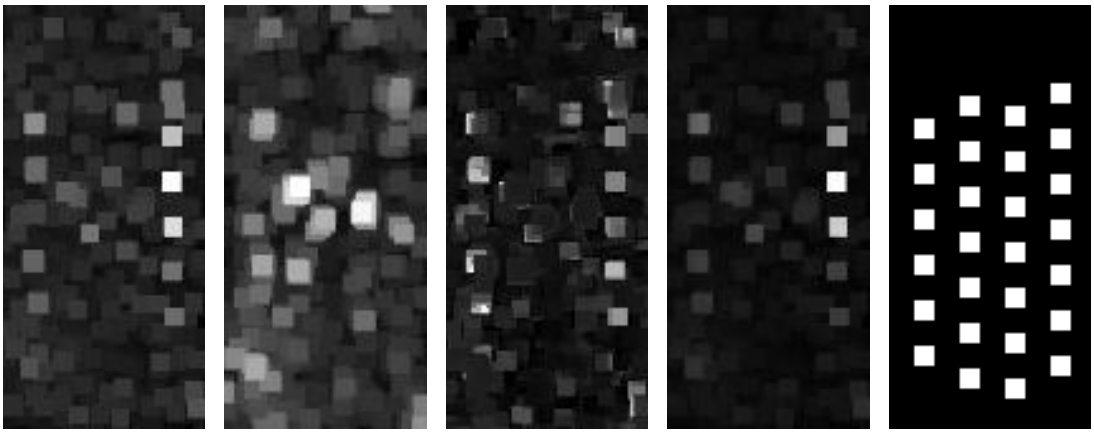

(a) (b) (c) (d) (e)

Figure 7. The results of the Hough transform for benefit function B, of the South section of the ferruginous lane are depicted in (a). The same result is given for the tophat filter in (b) as well as the result of the Mahalanobis (c) (logarithmically scaled) and Fisher (d) based classifiers for the combination of those two features. In (e) the ground truth of the section is given.

positive contrast for the sand, clay and peat lanes and a negative contrast for the ferruginous lane. There was negligible contrast for buried landmines in all lanes. In each lane the pattern of landmines is duplicated, resulting in two sections: North and South. One pattern of landmines consists of three landmine types: NR22/NR24 (identical except for color), PMN and M14, which have diameters between 5 and 12 cm. In a pattern three burial depths occur, at surface level (the top of the body of the landmine is laid at surface level), at one centimeter and at six centimeters below the surface. In both last mentioned cases the highest point of the landmine is used as a reference. Processing of this data is performed on the individual images rather then on the mosaics as presented in Figure 6.

3.2. Training and evaluation

For the training and evaluation processes we have been conducting two separate sets of experiments:

- In the first set of experiments we have split every test lane in a train and an evaluation part. Both parts contain the same landmine objects laid at the same depths.
- In the second set of experiments we again used the same split of each test lane. Here we performed training on half of one lane and all other full lanes, and evaluated on the other half of that lane. This leave-section-out scheme basically is a modified leave-one-out[17] evaluation scheme and is comparable to the leave-lane-out evaluation.[18]

The first set of experiments, based on training on the same soil type only as evaluating, should lead to better adjusted training results. The second set of experiments, based on training on several soil types, should result in more general training. As such it can be expected that in the second set of experiments the fall-back in performance of independent evaluation compared to the training results is less than the fall-back seen in the first set of experiments.

3.3. Single Lane results

Table 1 gives the results for the first set of experiments for the Hough transform and tophat filter methods. Each value is computed from eight results, as we have eight independent training and evaluation areas. It can be seen that the benefit can be negative for some evaluation values. This indicates that in those cases the system does not provide useful information.

Figure 7 shows the result of the Hough transform and the tophat filter as defined by benefit function B, for the South section of the ferruginous lane. Figure 8 shows the ROC curves for the Hough transform and tophat filter for training on the South section of the ferruginous lane. Here we see clearly that it is not possible to specify one optimal ROC curve, only with a well defined benefit function it is clear which ROC curve fits the application best.

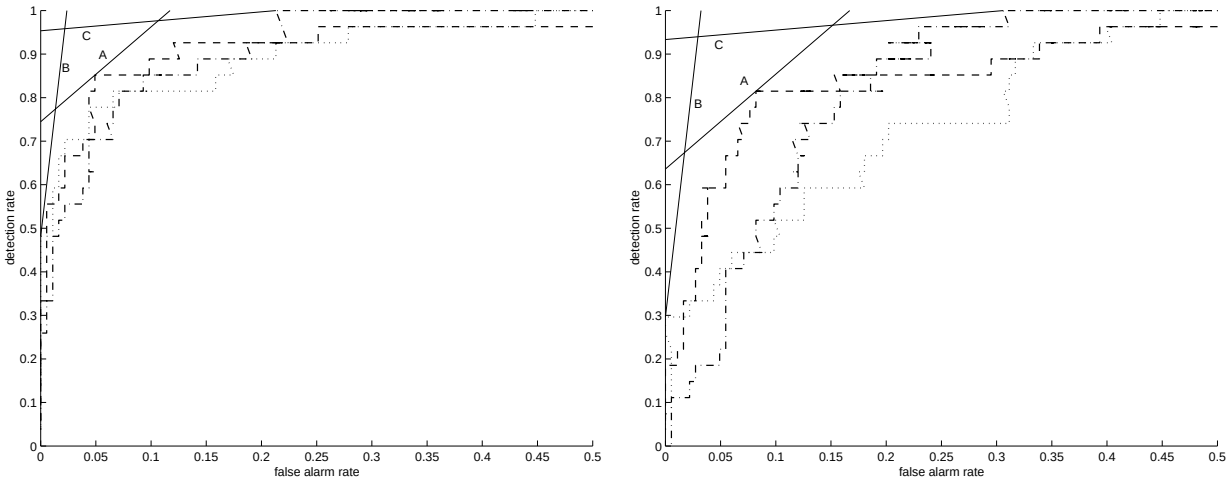

Figure 8. The optimal ROC curves of the Hough (a) transform and tophat (b) filter for the South section of the ferruginous lane. Also plotted are the iso-benefit lines for benefit functions A, B, and C touching at the optimal working point.

Table 1 also shows the results for the first set of experiments for the Mahalanobis feature selection method. It can be seen that the Mahalanobis feature selection method leads to less performance compared to the single feature performances. We believe this is the result of the fact that the Mahalanobis distance metric models the probability density function as a Gaussian function. The confidence values as produced by our Hough transform and tophat filter do not have a median value which represents maximum confidence for a landmine object, but instead increasing higher values represent increasing higher confidence. This means that scarce very high confidence value is erroneously considered 'background' by the Mahalanobis classifier while correctly be considered 'foreground' by the single feature threshold-based classifiers.

Also in Table 1 the results are given for the Fisher feature selection method. In contrast to the Mahalanobis method the Fisher method equals for all classifiers at least the single feature performances. In Table 1 also the number of features used for the optimal classifiers based on the Fisher metrics are shown. Here it can be seen that for many classifiers the Fisher metric selects only a single feature. Also, for those cases where multiple features are selected at least one of the selected features represents either the Hough transform or the tophat filter result for that same benefit function. In Figure 9 shows a scatter plot for the confidence levels as produced by the optimal Hough transform and tophat filter for benefit function B and their detection thresholds for the South section of the ferruginous lane. Also in this figure the results of the Mahalanobis and Fisher based classifiers are given.

3.4. Leave-section-out results

The Table 2 gives the performance in terms of benefit numbers for the second training and evaluation method. We see that the performance for the training sections is less than for the first set of experiments. This is logical as training has to be performed over a more diverse data set, leading to algorithms trained for generic object features rather than specifics of individual training objects. This is verified by the evaluation results: even though the training has been performed on soil types including others than the evaluation soil type, the fall-back in performance between training and evaluation is significant less compared to the first set of experiments. Especially for some classifiers we saw a huge performance decrease for the first set of experiments we now see only a moderate performance decreases. In Table 2 the number of features that are used for the optimal classifiers for the second experiments set based on the Fisher criterion are also shown.

4. CONCLUSIONS AND DISCUSSION

A large performance decrease can be observed between detection results as achieved on the training sets and those achieved on the independent evaluation sets. This indicates that the size of the training set is not sufficiently large to be representative of the full statistics of the phenomena encountered in the out-door test lanes. Considering the dimensions of the training set one can question the feasibility of a generalized classification system.

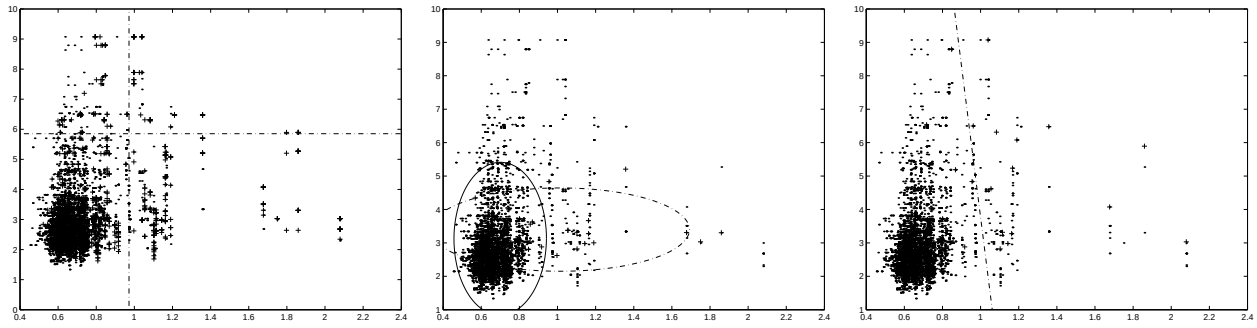

Figure 9. A scatter plot of the confidence values for the South section of the ferruginous lane as produced by the optimal Hough transform and tophat filter for benefit function B is given in (a), including the threshold values as found for the individual features. In (b) the ellipses representing the covariances of the Mahalanobis classifier using these two features is overlaid on the scatter plot of the background and selected landmine representations for the Mahalanobis distance. In (c) is plotted the decision line for the Fisher discriminant for these features overlaid on the scatter plot of background and Fisher landmine representations.

It also means that, although we only train with four free parameters for both the Hough transform and the tophat filter, we have too much free parameters in our algorithms, leading to training to specifics of the objects in the data set rather then training to the generics of the image forming process of the objects and backgrounds under study.

The classifier based on the Mahalanobis distance often performs less than classification using the confidence levels of either the Hough transform or the tophat filter. We expect this to be related to the erroneous assumption within the Mahalanobis distance that the confidence levels are Gaussian distributed for both foreground and background class.

The Fisher linear discriminant equals or outperform the individual detectors on the training sets. This is not surprising as using a single of the decision levels thresholded by the individual detectors can be used as the only input to Fisher linear discriminant, which on a single input feature also acts as a threshold. As such the Fisher linear discriminant is a superset of the individual detectors.

In the comparison between the first and the second set of experiments it can be seen that, although the benefit values for the evaluation are lower than those in the first set of experiments, the fall-back in performance for the second set of experiments is much lower. Where in the first set of experiments the benefit for the evaluation result often was negative (indicating that the method does not add value), the second set of experiments in majority shows positive evaluation benefits. This means that extending the training set with less representative training data did result in more robust evaluation results.

For the benefit function B, and to a lesser extend for benefit functions A and C, the performance of the leave-section-out method is lower. This is explained by the fact that the parameterization used is not normalized for each lane.

For both the Hough transform and the tophat filter, there is not one parameter setting that has optimal benefit for all benefit functions.

5. RECOMMENDATIONS

This fall-back in performance observed between training and evaluation probably is related to the optimization method utilized. In these experiments we selected those parameters having the optimal performance on the training set. Instead a scheme could be followed where the complete data set is separated into a training, selection and evaluation set. Then training can be done on the training set, selection of best parameters on the selection set, and independent evaluation of the result on the evaluation set. We expect that this will lead to more robust parameter settings.

The methodology used in this paper to condense the grid cells labelled foreground in the ground truth to true object representatives is *ad hoc* and does not necessarily lead to optimal trained classifiers.

To improve the performance of the leave-section-out method it is suggested to use a parameterization that is normalized for soil type and meteorological conditions.

		Benefit function A		Benefit function B		Benefit function C	
		training	evaluation	training	evaluation	training	evaluation
Hough	Average	0.65030	0.32507	0.43320	-0.36376	0.77508	-0.31595
	St. Dev.	0.05026	0.21676	0.05710	0.87761	0.04794	0.88877
Tophat	Average	0.66501	0.41601	0.39153	-0.97553	0.75732	0.00978
	St. Dev.	0.02978	0.09855	0.10182	1.91764	0.04664	0.63708
Mahalanobis	Average	0.65493	0.33383	0.38690	-1.09821	0.75383	-0.06293
	St. Dev.	0.06518	0.16687	0.07991	1.96847	0.06685	0.86961
	Avg. Feat.	$1\frac{3}{8}$		$2\frac{3}{4}$		$2\frac{1}{8}$	
Fisher	Average	0.68684	0.40526	0.47685	-0.87533	0.80445	-0.30161
	St. Dev.	0.04126	0.09639	0.06982	1.95314	0.03288	0.90281
	Avg. Feat.	$1\frac{1}{8}$		$1\frac{3}{8}$		$1\frac{1}{4}$	

Table 1. Results for the different methods, for training and evaluation on a single lane. Shown are the average and standard deviation of the benefit over the eight training and evaluation sets. For the two feature selection methods the average number of features used in the combination with the most benefit is also shown.

		Benefit function A		Benefit function B		Benefit function C	
		training	evaluation	training	evaluation	training	evaluation
Hough	Average	0.46495	0.37483	0.25761	0.15509	0.48615	0.27768
	St. Dev.	0.01420	0.09420	0.01521	0.17705	0.01110	0.29053
Tophat	Average	0.43497	0.35847	0.18164	0.00661	0.49360	0.36769
	St. Dev.	0.01514	0.16692	0.02916	0.19513	0.02147	0.37464
Mahalanobis	Average	0.45682	0.33003	0.02414	-0.03538	0.51860	0.41201
	St. Dev.	0.02215	0.11920	0.01279	0.13108	0.01834	0.12422
	Avg. Feat.	$1\frac{7}{8}$		$4\frac{1}{4}$		2	
Fisher	Average	0.46946	0.35880	0.25997	0.02943	0.51480	0.26531
	St. Dev.	0.01673	0.11202	0.01753	0.34273	0.03370	0.15397
	Avg. Feat.	$1\frac{1}{8}$		$1\frac{1}{8}$		$1\frac{5}{8}$	

Table 2. Results for the different methods, for training on seven sections and evaluation on the left out section. Shown are the average and standard deviation of the benefit over the eight training and evaluation sets. For the two feature selection methods the average number of features used in the combination with the most benefit is also shown.

ACKNOWLEDGMENTS

This paper describes work partly funded by the European Commission as ESPRIT project LOTUS, number 29812.

We gratefully acknowledge the discussions in Task Group NATO RTO SET-035/RTG19 ”Systems Level Fusion for Land Surveillance” on usefull system evaluation methodologies.

REFERENCES

1. W. de Jong, H. A. Lensen, and Y. H. L. Janssen. Sophisticated test facility to detect land mines. In A. C. Dubey and J. F. Harvey, editors, *Proc. SPIE Vol. 3710, Detection and Remediation Technologies for Mines and Minelike Targets IV*, pages 1409–1418, Orlando (FL), USA, Apr. 1999.
2. J. G. M. Schavemaker, F. Cremer, K. Schutte, and E. den Breejen. Infrared processing and sensor fusion for anti-personnel land-mine detection. In *Proceedings of IEEE Student Branch Eindhoven: Symposium Imaging*, pages 61–71, Eindhoven, the Netherlands, May 2000.
3. J. G. M. Schavemaker, E. den Breejen, F. Cremer, K. Schutte, and K. W. Benoist. Depth fusion for anti-personnel landmine detection. In A. C. Dubey, J. F. Harvey, J. T. Broach, and V. George, editors, *Proc. SPIE Vol. 4394, Detection and Remediation Technologies for Mines and Minelike Targets VI*, pages 1071–1081, Orlando (FL), USA, Apr. 2001.
4. Y. H. L. Janssen, A. N. de Jong, H. Winkel, and F. J. M. van Putten. Detection of surface laid and buried mines with IR and CCD cameras, an evalutation based on measurements. In A. C. Dubey, R. L. Barnard, and C. J. Lowe, editors, *Proc. SPIE Vol. 2765, Detection and Remediation Technologies for Mines and Minelike Targets*, pages 448–459, Orlando (FL), USA, Apr. 1996.

5. F. Cremer, W. de Jong, K. Schutte, J. T. Johnson, and B. A. Baertlein. Surface mine signature modeling for passive polarimetric IR. In J. T. Broach, R. S. Harmon, and G. J. Dobeck, editors, *Proc. SPIE Vol. 4742, Detection and Remediation Technologies for Mines and Minelike Targets VII*, Orlando (FL), USA, Apr. 2002.
6. S.-H. Hong, T. Miller, B. Borchers, J. M. H. Hendrickx, J. Simunek, H. A. Lensen, P. B. W. Schwering, and B. A. Baertlein. Landmine detection in bare soils using thermal infrared sensors. In J. T. Broach, R. S. Harmon, and G. J. Dobeck, editors, *Proc. SPIE Vol. 4742, Detection and Remediation Technologies for Mines and Minelike Targets VII*, Orlando (FL), USA, Apr. 2002.
7. V. Leavers. *Shape Detection in Computer Vision Using the Hough Transform*. Springer-Verlag, 1992.
8. P. Verbeek and L. van Vliet. Estimators of 2D edge length and position, 3D surface area and position in sampeled grey-valued images. *BioImaging*, 1(1):47–61, 1993.
9. J. Egan. *Signal Detection Theory and ROC analysis*. Series in Cognition and Perception. Academic Press, 1975.
10. P. Soille. *Morphologische Bildverarbeitung, Grundlagen, Methoden, Anwendungen*. Springer, 1998.
11. J. Damon. Properties of ridges and cores for 2-D images. *Journal of Mathematical Imaging and Vision*, 10(2):163–174, 1999.
12. E. den Breejen, K. Schutte, and F. Cremer. Sensor fusion for anti personnel landmine detection, a case study. In A. C. Dubey and J. F. Harvey, editors, *Proc. SPIE Vol. 3710, Detection and Remediation Technologies for Mines and Minelike Targets IV*, pages 1235–1245, Orlando (FL), USA, Apr. 1999.
13. F. Provost and T. Fawcett. Robust classification systems for imprecise environments. pages 706–713, Madison (WI), USA, July 1998.
14. Final Report of NATO RTO SET-035/RTG19 "Systems Level Fusion for Land Surveillance". A method for evaluating the relative military benefit of sensor fusion. Technical report, NATO RTO, To be published 2002.
15. F. Cremer, K. Schutte, J. G. M. Schavemaker, and E. den Breejen. A comparision of decision-level sensor-fusion methods for anti-personnel landmine detection. *Information Fusion*, 2(3):187–208, Sept. 2001.
16. K. Fukunaga. *Introduction to statistical pattern recognition*. Academic press, Inc., Boston, USA, 2 edition, 1990.
17. K. Fukunaga and D. Hummels. Estimation of classifier performance. *IEEE*, 11(10):1087–1101, 1989.
18. F. Cremer, J. G. M. Schavemaker, E. den Breejen, and K. Schutte. Towards an operational sensor fusion system for anti-personnel landmine detection. In A. C. Dubey, J. F. Harvey, J. T. Broach, and R. E. Dugan, editors, *Proc. SPIE Vol. 4038, Detection and Remediation Technologies for Mines and Minelike Targets V*, pages 792–803, Orlando (FL), USA, Apr. 2000.